

Predictive Direct Control of Permanent Magnet Assisted Bearingless Synchronous Reluctance Motor Based on Super Twisting Sliding Mode

Min Gao*, Huangqiu Zhu, and Yijian Shi

Abstract—In order to solve the problem of the low accuracy of permanent magnet assisted bearingless synchronous reluctance motor (PMa-BSynRM) direct control, the predictive control is applied to direct control of the PMa-BSynRM. Meanwhile, in view of the disadvantages of high ripple (torque ripple, flux linkage ripple) and poor robustness in traditional predictive direct control (PDC), a fractional super twisting sliding mode controller (FSTMC) is proposed. Firstly, the mathematical models of torque and radial suspension force of the PMa-BSynRM are derived. Secondly, the torque and flux controller based on the FSTMC are designed, and the stability of the FSTMC is verified. Thirdly, the torque predictive controller and suspension force predictive controller are designed, and the algorithm of PDC is described. Finally, the FSTMC-PDC system of the PMa-BSynRM is built and simulated by Matlab/Simulink module. The simulated and experimental results confirm the validity and superiority of the proposed method.

1. INTRODUCTION

A permanent magnet assisted bearingless synchronous reluctance motor (PMa-BSynRM) [1] is a new research field of bearingless motor. It integrates a permanent magnet assisted synchronous reluctance motor, a synchronous reluctance motor (PMa-SynRM), and bearingless technology. Therefore, the PMa-BSynRM not only has the advantages of high power factor, simple structure, and low cost, but also inherits the advantages of no contact, no lubrication, no pollution, long life, etc. [2]. It can be widely used in aerospace, biomedicine, semiconductor industry, etc. Hence, in recent years, the PMa-BSynRM drive control has become a hot research topic.

Generally speaking, the main control strategies employed for the high performance control of PMa-BSynRM drives are field oriented control (FOC) using space vector pulse width modification (SVPWM) [3] and direct control (direct torque control and direct suspension force control) [4, 5]. Compared with FOC, direct control has the advantages of simple controller structure, less coordinate transformation, and fast dynamic response, and the direct control is applied to the PMa-BSynRM drive. However, the control accuracy is low due to the signal detection and transmission delay in the direct control, which greatly reduces the control accuracy and response speed. By predicting the torque and flux at a certain time, the model predictive control calculates the convergent flux at the next time to select the voltage vector of the next control period, which can solve the problem of transmission delay well. Therefore, this paper focuses on the prediction direct control (PDC) [6].

The prediction function of PDC is mainly reflected in the prediction of torque, flux linkage, and suspension force, while hysteresis comparator is still used in the output control signal. This will cause the torque and flux linkage to have an error band, which brings the disadvantages of torque ripple, flux

Received 15 March 2021, Accepted 26 April 2021, Scheduled 27 April 2021

* Corresponding author: Min Gao (ujseeqm1801@126.com).

The authors are with the School of Electrical and Information Engineering, Jiangsu University, Zhenjiang 212013, China.

linkage ripple, and suspension force ripple. Many researchers have proposed solutions [7–10]. In [7], a zero voltage vector based PDTC-PWM control method is proposed, which considers the back EMF and decoupling components in the voltage vector selection to improve the control performance. In [8], a composite torque regular based DTC scheme is proposed. However, most of these control methods sacrifice the robustness of the system. Hence, the PDC based on a sliding mode controller to replace hysteresis comparator is proposed [11–14]. In [12], nonlinear-robust control approaches are applied in sliding mode. A sliding mode controller based on a new reaching law is developed for designing a sliding mode speed controller (SMSC) for the DTC system in [13]. However, sliding mode control has the characteristics of strong robustness, but also causes system chattering, which hinders its application in practical engineering. In this way, super twisting sliding mode control is introduced, which can improve the chattering problem in sliding mode control [15].

To improve the control accuracy and robustness of the PMA-BSynRM direct control, a predictive direct control based on a fractional super twisting sliding mode controller (FSTMC-PDC) is proposed. The fractional super twisting sliding mode controller is designed instead to realize the function of hysteresis comparison. The convergence and stability of the FSTMC are proved. The torque prediction controller and suspension force prediction controller are designed to construct a predictive direct control system based on FSTMC of the PMA-BSynRM. By Matlab/Simulink simulation, the correctness and effectiveness of the control strategy are verified. Finally, the experimental platform is built to verify the effectiveness of the proposed method.

2. OPERATION PRINCIPLE AND MATHEMATICAL MODELS OF THE PMA-BSYNRM

2.1. Operation Principle of the PMA-BSynRM

The PMA-BSynRM topology studied in this paper is shown in Figure 1(a). On the premise of ensuring the best performance of the PMA-BSynRM, the motor still has the advantage of simple structure, and the numbers of slots and poles are selected as 24 and 4. The stator of the motor adopts pear groove, and two sets of windings are embedded in the stator slot: the outer winding is torque windings, and the inner winding is suspension force windings. The rotor structure of the motor no longer adopts the traditional salient type, but adopts flux barriers, and inserts the permanent magnets in the rotor to obtain a larger salient ratio and power factor. Therefore, the torque and suspension force performance of the motor are improved.

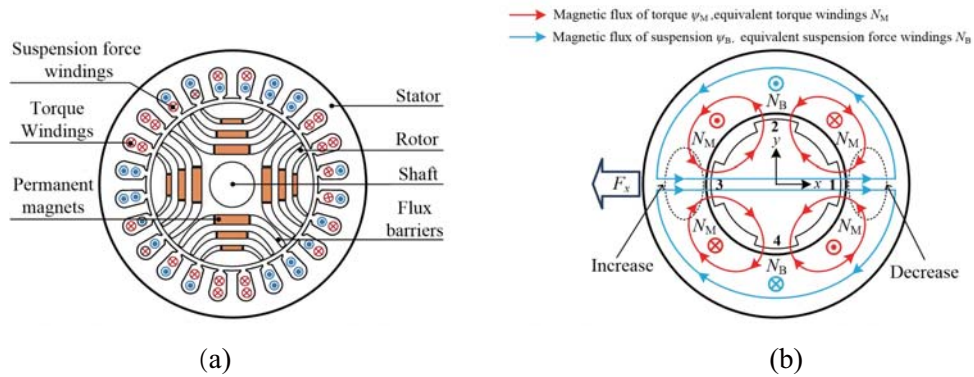


Figure 1. Topology and operation principle of PMA-BSynRM. (a) topology of PMA-BSynRM. (b) the principle of the radial suspension force generation of PMA-BSynRM.

The stable suspension condition of the rotor of PMA-BSynRM is the difference between pole pair of torque windings (P_M) and pole pair of suspension force windings (P_B), which is 1. In this paper, the pole pair of torque windings is 1, and the pole pair of suspension force windings is 2, which satisfies the above conditions. Figure 1(b) shows the principle of generating the suspension force in the x axis of the

PMA-BSynRM. When the torque windings and suspension force windings are excited by the current at the same time, the flux density of air gap 3 will increase, and the flux density of air gap 4 will decrease by changing the current phase angle. Therefore, due to the action of the superimposed magnetic field, the suspension force F_x acts on the rotor in the positive direction of the x axis. To generate suspension force in other directions can be achieved by changing the current phase angle.

2.2. Mathematical Models of the PMA-BSynRM

The mathematical model of the PMA-BSynRM torque subsystem is similar to the traditional synchronous reluctance motor. In a static α - β reference frame, a PMA-BSynRM model with stator current and stator flux linkages as stated can be described as

$$\begin{cases} Di_{M\alpha} = -\frac{R_M}{L_{Md}}i_{M\alpha} - \omega_r \frac{L_{Md} - L_{Mq}}{L_{Md}}i_{M\beta} + e_\alpha + \frac{1}{L_{Md}}u_{M\alpha} \\ Di_{M\beta} = -\frac{R_M}{L_{Md}}i_{M\beta} + \omega_r \frac{L_{Md} - L_{Mq}}{L_{Md}}i_{M\alpha} + e_\beta + \frac{1}{L_{Md}}u_{M\beta} \\ D\psi_{M\alpha} = -R_M i_{M\alpha} + u_{M\alpha} \\ D\psi_{M\beta} = -R_M i_{M\beta} + u_{M\beta} \end{cases} \quad (1)$$

where D is the differential operator; $u_{M\alpha}$ and $u_{M\beta}$ are torque windings stator voltages in α - and β -axes respectively; $i_{M\alpha}$ and $i_{M\beta}$ are torque winding stator currents in α - and β -axes, respectively; $\psi_{M\alpha}$ and $\psi_{M\beta}$ are torque windings stator flux linkages in α - and β -axes, respectively; L_{Md} and L_{Mq} are inductances in d - and q -axes, respectively; R_M is the resistance of torque windings; e_α and e_β are torque winding expansions of the back-EMF in α - and β -axes, respectively; ω_r is the rotor electrical angular velocity.

The electromagnetic torque and stator flux linkage can be obtained as

$$\begin{cases} T_e = \frac{3}{2}P_M(\psi_{M\alpha}i_{M\beta} - \psi_{M\beta}i_{M\alpha}) \\ |\psi_M| = \sqrt{\psi_{M\alpha}^2 + \psi_{M\beta}^2} \\ \lambda_M = \arctan(\psi_{M\beta}/\psi_{M\alpha}) \end{cases} \quad (2)$$

According to the principle of radial suspension force generation of PMA-BSynRM, Maxwell tensor method is used to deduce the expressions of Maxwell force F_α and F_β in

$$\begin{cases} F_\alpha = k_{M1}\psi_{m1}\psi_{m2} \cos(\lambda - \mu) + k_{M2}\psi_{m1}\psi_{m2} \cos(\lambda + \mu - 2\theta) \\ F_\beta = k_{M1}\psi_{m1}\psi_{m2} \sin(\lambda - \mu) + k_{M2}\psi_{m1}\psi_{m2} \sin(\lambda + \mu - 2\theta) \end{cases} \quad (3)$$

where $k_{m1} = \pi/27N_1N_2lr\mu_0$, $k_{m2} = \sqrt{3}/18N_1N_2lr\mu_0$, N_1 and N_2 are the turns of torque windings and suspension force windings, respectively; μ_0 is the air gap length; r is the radius of rotor; l is the length of the motor core; ψ_{m1} and ψ_{m2} are synthetic flux linkages of torque windings and suspension force windings respectively; λ is the phase angle of flux linkage in torque windings; μ is the phase angle of flux linkage in suspension force windings; θ is the electrical angle of motor.

In formula (3), the Maxwell force of the motor consists of two parts. One is the controllable suspension force produced by the current excitation of the suspension force windings (the first term), and the other is the uncontrollable unilateral magnetic pull force (the second term). Because the control strategy of suspension force is studied in this paper, the second item is not discussed.

3. DESIGN OF PREDICTIVE DIRECT CONTROLLER OF PMA-BSYNRM

3.1. Design of Fractional order Super twisting Sliding Mode Controller

The super twisting sliding mode algorithm is developed under the background of high order sliding mode variable structure theory. Its main idea is to apply the switch action to the high order derivative, not to the first derivative like the traditional sliding mode. In this way, the chattering problem of

the PMa-BSynRM control system can be effectively eliminated. In order to design a robust hysteresis comparator, a linear second order sliding mode controller [17] is used as

$$\begin{cases} y = g_1 |x_1|^r \operatorname{sgn}(x_1) + g_3 x_1 + x_2 \\ \frac{dx_2}{dt} = g_2 \operatorname{sgn}(x_1) + g_4 x_1 \end{cases}, \begin{cases} g_2(4g_4 + 8g_3^2) > g_1^2 g_3^2 \\ g_2 + g_1^2 > 0 \end{cases} \quad (4)$$

where x_1 is the designed sliding mode surface; g_1, g_2, g_3, g_4 , and g_5 are the sliding mode gains.

When a sliding mode controller is designed, the selection of approach law reflects the way that the system reaches the sliding mode surface. Generally speaking, when the system is away from the sliding mode surface, it is hoped to increase its rate, while when the system is close to the sliding mode surface, it is hoped that the speed will be as low as possible to reduce the harm caused by chattering. Therefore, the fractional approximation law is chosen here, which is faster and smoother than the traditional exponential approximation law. The fractional approximation law [18] is given as follows:

$$D^m S_I = -k S_I - \varepsilon \cdot \operatorname{sgn}(S_I) \quad (5)$$

where S_I is the sliding mode surface, sgn the symbolic function, k, ε the coefficient of fractional approximation law, $k > 0, \varepsilon > 0, m$ the integral coefficient of fractional order, and $0 < m < 1$.

The sliding mode surface S_I is constructed by introducing fractional integral. In addition, the time of approaching motion can be reduced by selecting appropriate parameters, and the flexibility and convergence speed of the control system can be improved. The sliding surface S_I [18] is defined as

$$S_I = \begin{bmatrix} S_{IT_e} \\ S_{I\psi_M} \end{bmatrix} = \begin{bmatrix} \tilde{T}_e + c_1 \cdot D^{-m} \\ \tilde{\psi}_M + c_2 \cdot D^{-m} \end{bmatrix} \quad (6)$$

where $\tilde{T}_e = T_e^* - T_e$, where T_e^* is the torque given value and T_e the torque actual value; $\tilde{\psi}_M = \psi_M^* - \psi_M$, where ψ_M^* is the flux linkages given value and ψ_M the flux linkages actual value; c_1, c_2 are fractional integral coefficients and $c_1 > 0, c_2 > 0$.

Based on Eq. (4), the torque and flux linkage FSTSM controller of PDTC are

$$\begin{cases} y_{T_e} = g_1 |S_{IT_e}|^r \operatorname{sgn}(S_{IT_e}) + g_3 S_{IT_e} + \int g_2 \operatorname{sgn}(S_{IT_e}) + g_4 S_{IT_e} dt \\ y_{\psi_M} = g_1 |S_{I\psi_M}|^r \operatorname{sgn}(S_{I\psi_M}) + g_3 S_{I\psi_M} + \int g_2 \operatorname{sgn}(S_{I\psi_M}) + g_4 S_{I\psi_M} dt \end{cases} \quad (7)$$

The Lyapunov function $V = (S_I^T * S_I)/2$ greater than 0 is selected to verify the stability of the sliding mode surface, thus can be derived as

$$\dot{V} = S_I^T \cdot \dot{S}_I \quad (8)$$

Substituting Eq. (1) into Eq. (8) yields

$$\begin{aligned} \dot{V} &= S_I^T \cdot \dot{S}_I \\ &= S_I^T \cdot \begin{Bmatrix} -\frac{3}{2} P_M \{ D\psi_{M\alpha} i_{M\beta} + \psi_{M\alpha} D i_{M\beta} - D\psi_{M\beta} i_{M\alpha} - \psi_{M\beta} D i_{M\alpha} \} \\ -2\psi_{M\alpha} D\psi_{M\alpha} - 2\psi_{M\beta} D\psi_{M\beta} \end{Bmatrix} \end{aligned} \quad (9)$$

$$\text{where } A = \begin{bmatrix} A_1 \\ A_2 \end{bmatrix} = \begin{bmatrix} -\frac{3}{2} P_M \left\{ \frac{\psi_{M\alpha}(L_{Md} - L_{Mq})\omega_r i_{M\alpha} - R_M i_{M\beta} - e_\beta}{L_{Md}} + \frac{\psi_{M\beta}(L_{Md} - L_{Mq})\omega_r i_{M\beta} + R_M i_{M\alpha} + e_\alpha}{L_{Md}} \right\} \\ 2\psi_{M\alpha} R_M i_{M\alpha} + 2\psi_{M\beta} R_M i_{M\beta} \end{bmatrix},$$

$$B = \begin{bmatrix} B_1 \\ B_2 \end{bmatrix} = \begin{bmatrix} c_1 \cdot D^{-m+1} \tilde{T}_e \\ c_2 \cdot D^{-m+1} \tilde{\psi}_s \end{bmatrix}, \quad C = \begin{bmatrix} -\frac{3}{2} P_M \left\{ i_{M\beta} - \frac{\psi_{M\beta}}{L_{Md}} \right\} & -\frac{3}{2} P_M \left\{ \frac{\psi_{M\alpha}}{L_{Md}} - i_{M\alpha} \right\} \\ -2\psi_{M\alpha} & -2\psi_{M\beta} \end{bmatrix}.$$

According to Eq. (4), y and S_I satisfy the following inequalities

$$\begin{cases} S_{IT_e} * y_{T_e} = S_{IT_e} \left\{ g_1 |S_{IT_e}|^r \operatorname{sgn}(S_{IT_e}) + g_3 S_{IT_e} + \int g_2 \operatorname{sgn}(S_{IT_e}) + g_4 S_{IT_e} dt \right\} \geq 0 \\ S_{I\psi_M} * y_{\psi_M} = S_{I\psi_M} \left\{ g_1 |S_{I\psi_M}|^r \operatorname{sgn}(S_{I\psi_M}) + g_3 S_{I\psi_M} + \int g_2 \operatorname{sgn}(S_{I\psi_M}) + g_4 S_{I\psi_M} dt \right\} \geq 0 \end{cases} \quad (10)$$

Substituting Eqs. (10) and (9) into Eq. (8) yields

$$\dot{V} = S_1^T \cdot \dot{S}_1 < 0 \quad (11)$$

According to the above derivation, it can be seen that the system can reach the equilibrium state in any initial state, and the system meets the stability condition. The design process of sliding mode controller of suspension force subsystem is similar to the above process.

3.2. Predictive Direct Torque Control of PMA-BSynRM

Predictive direct control is the combination of predictive control and DTC. The main idea is: after obtaining the initial values of flux $\psi(k)$, torque $T(k)$ and suspension force $F(k)$ at $(k)T_s$, $\psi(k+1)$, $T(k+1)$ and $F(k+1)$ at $(k+1)T_s$ are further predicted. Then, the suitable voltage vectors $v_1(k+1)$ and $v_2(k+1)$ are calculated and applied at $(k+1)T_s$. In this way, the closed loop feedback of the system is compensated, and the adverse effects of system sampling and transmission delay are improved. Figure 2 shows the structure block diagram of torque subsystem prediction controller, including Clark coordinate transformation module, flux observer module, model prediction module of current, torque, and torque winding flux linkage.

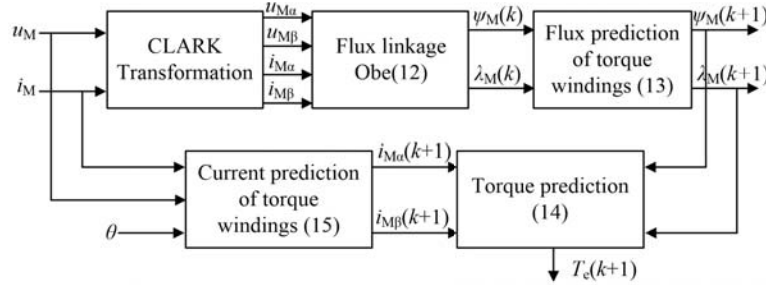


Figure 2. Predictive controller of torque subsystem.

Generally, the precision of the electromagnetic torque and stator flux linkage observer is very important. In [16], a stator flux observer based on the phase-locked loop principle is proposed. The flux linkage observer of torque windings is

$$\begin{cases} \psi_{Ma} = (u_{Mg} \cdot \cos \theta_f) / (G(s) \cdot \theta_e) \\ \psi_{Mb} = (u_{Mg} \cdot \sin \theta_f) / (G(s) \cdot \theta_e) \\ |\psi_M| = \sqrt{\psi_{Ma}^2 + \psi_{Mb}^2} \\ \lambda_M = \arctan(\psi_{Mb} / \psi_{Ma}) \end{cases} \quad (12)$$

where $G(s)$ is the transfer function of flux observer, and it can be found in [16]; θ_f is the phase of input voltage.

The main function of the prediction module is to discretize the motor model and establish the prediction model of the output signal at the next time. Therefore, the flux amplitude $\psi_M(k+1)$ and electromagnetic torque $T_e(k+1)$ of torque winding of PMA-BSynRM are as follows

$$\begin{cases} \psi_{Ma}(k+1) = \psi_{Ma}(k) + [u_{Ma} - R_M i_{Ma}(k)] T_s \\ \psi_{Mb}(k+1) = \psi_{Mb}(k) + [u_{Mb} - R_M i_{Mb}(k)] T_s \\ |\psi_M(k+1)| = \sqrt{\psi_{Ma}^2(k+1) + \psi_{Mb}^2(k+1)} \\ \lambda_M(k+1) = \arctan \frac{\psi_{Mb}(k+1)}{\psi_{Ma}(k+1)} \end{cases} \quad (13)$$

$$T_e(k+1) = \frac{3P_M}{2} [\psi_{Ma}(k+1)i_{Mb}(k+1) - \psi_{Mb}(k+1)i_{Ma}(k+1)] \quad (14)$$

From formula (16), the calculation of torque also needs the prediction model of current. By discretizing the PMA-BSynRM voltage and current equation, the current prediction model of torque winding in d-q reference frame is derived as

$$\begin{cases} i_{M_d}(k+1) = i_{M_d}(k) + \frac{u_{M_d} - R_M i_{M_d}(k) + \omega(k) L_{M_d} i_{M_q}(k)}{L_{M_d}} T_s \\ i_{M_q}(k+1) = i_{M_q}(k) + \frac{u_{M_q} - R_M i_{M_q}(k) - \omega(k) \psi_f - \omega(k) L_{M_d} i_{M_d}(k)}{L_{M_q}} T_s \\ |i_{M_d}(k+1)| = \sqrt{(i_{M_d}(k+1))^2 + (i_{M_q}(k+1))^2} \end{cases} \quad (15)$$

The real time angular position detected by Hall sensor is input into the current prediction model, and the current prediction value at $(k+1)T_s$ in α - β coordinate system can be obtained by park inverse transformation. The electromagnetic torque error and flux linkage error are input into the FSTSMC controller designed in Section 3.1 to obtain the space voltage of the torque subsystem.

3.3. Predictive Direct Suspension Force Control of PMA-BSynRM

Similar to torque prediction control, the core of suspension force prediction control is a suspension force subsystem prediction controller. Its structure block diagram is shown in Figure 3., including coordinate Clark transformation module, flux observer module, prediction module of suspension force windings flux linkage, torque windings synthetic air-gap flux linkage, and radial suspension force.

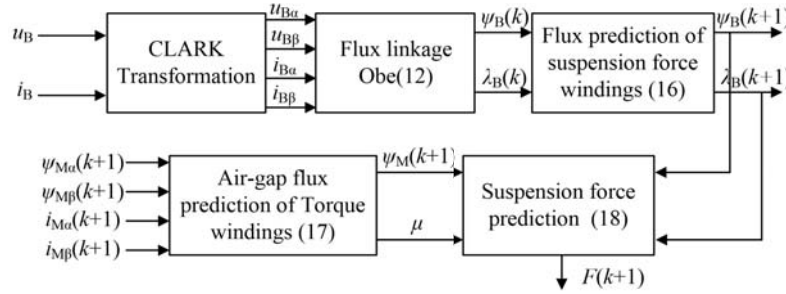


Figure 3. Predictive controller of suspension force subsystem.

Similar to Eq. (15), the flux amplitude $\psi_\beta(k+1)$ and phase $\lambda_\beta(k+1)$ of suspension force windings at $(k+1)T_s$ are

$$\begin{cases} \psi_{B\alpha}(k+1) = \psi_{B\alpha}(k) + [u_{B\alpha} - R_B i_{B\alpha}(k)] T_s \\ \psi_{B\beta}(k+1) = \psi_{B\beta}(k) + [u_{B\beta} - R_B i_{B\beta}(k)] T_s \\ |\psi_B(k+1)| = \sqrt{\psi_{B\alpha}^2(k+1) + \psi_{B\beta}^2(k+1)} \\ \lambda_B(k+1) = \arctan \frac{\psi_{B\beta}(k+1)}{\psi_{B\alpha}(k+1)} \end{cases} \quad (16)$$

In the process of motor operation, the influence of windings leakage must be considered. The amplitude and phase of torque windings synthetic air-gap flux linkage are

$$\begin{cases} \psi_{m\alpha}(k+1) = \psi_{M\alpha}(k+1) - L_{M\delta} i_{M\alpha}(k+1) \\ \psi_{m\beta}(k+1) = \psi_{M\beta}(k+1) - L_{M\delta} i_{M\beta}(k+1) \\ |\psi_m(k+1)| = \sqrt{\psi_{m\alpha}^2(k+1) + \psi_{m\beta}^2(k+1)} \\ \mu(k+1) = \arctan \frac{\psi_{m\beta}(k+1)}{\psi_{m\alpha}(k+1)} \end{cases} \quad (17)$$

Substituting Eqs. (18) and (19) into Eq. (3), the prediction model of suspension force of PMA-BSynRM is

$$\begin{cases} F_{\alpha}(k+1) = k_{M1}\psi_{m1}(k+1)\psi_B(k+1)\cos[\mu(k+1) - \lambda_B(k+1)] \\ F_{\beta}(k+1) = k_{M1}\psi_{m1}(k+1)\psi_B(k+1)\sin[\mu(k+1) - \lambda_B(k+1)] \end{cases} \quad (18)$$

The suspension force error is input into the FSTSMC controller designed in Section 3.1 to obtain the space voltage of the suspension force subsystem. Then, the switching signal of the drive voltage inverter is output by SVPWM modulation, and the direct suspension force control of the PMA-BSynRM is formed by the output of the inverter, which is used for the stable operation and suspension of the motor.

4. SIMULATION TEST

The predictive direct control system for PMA-BSynRM based on fractional super twisting sliding mode controller is designed by combining torque and suspension force predictive direct torque control subsystems. The control block diagram is shown in Figure 4. FSTMC is used to replace the hysteresis comparator in the traditional direct control. Different from the traditional direct control, the torque error and flux error are fed into the FSTMC, to calculate the space voltage vector through the FSTMC. The simulation based on Matlab/simulink is carried out to verify the effectiveness of the proposed control strategy, and the simulation results are analyzed.

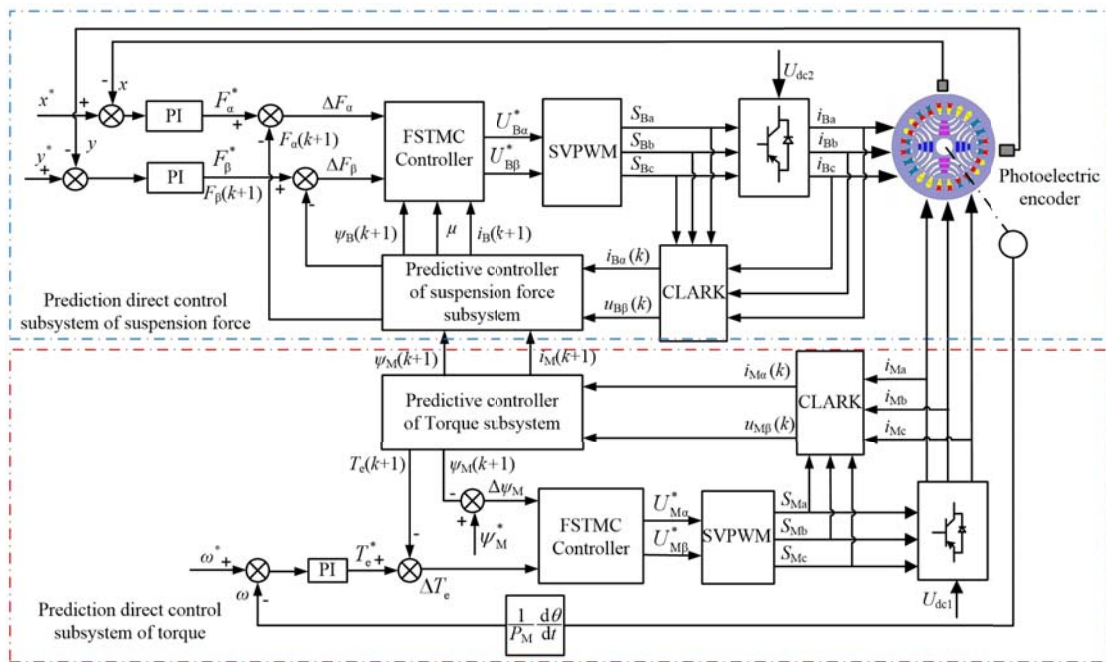


Figure 4. Block diagram of PMA-BSynRM predictive direct control system based on FSTMC.

Operating conditions: given speed 3000 r/min at $t = 0.4$ s, load from N·m to 1.5 N·m at $t = 0.2$ s, initial rotor position (0.2 mm, 0.2 mm), Figure 5 shows the speed response of the proposed FSTMC-PDC and PDC with traditional hysteresis control. Form Figure 5(b), the speed response is fast; the given speed can be reached quickly; and the waveform is smooth. In Figure 5(a), the speed also reaches the given speed in the specified time, but the speed waveform fluctuates greatly, which has a certain effect on the stable operation of the PMA-BSynRM.

Figure 6 shows the FSTMC-PDC and PDC flux trajectory comparison. As can be seen, the flux trajectory of FSTMC-PDC is relatively smooth, and the trajectory accords with the theoretical circle. Because of the hysteresis comparator, the output space voltage vector of PDC is discontinuous, and the flux trajectory has a gap. Figure 7 shows the torque response comparison between FSTMC-PDC and

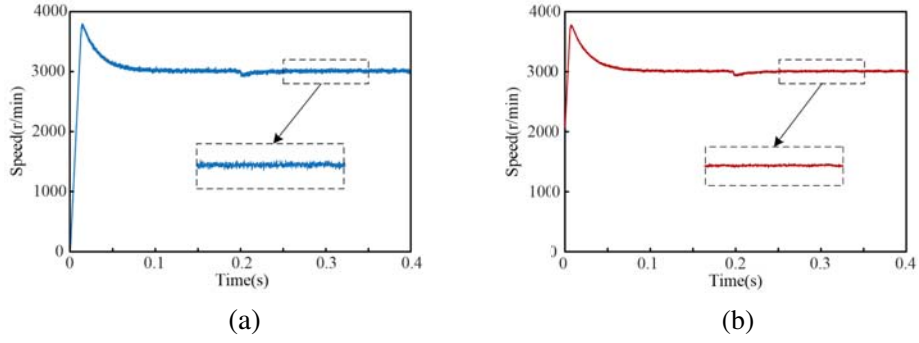


Figure 5. Speed waveforms in two methods. (a) PDC. (b) FSTMC-PDC.

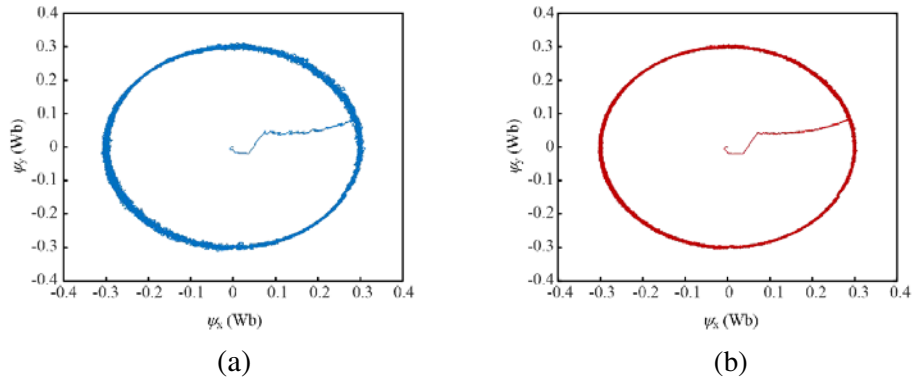


Figure 6. Flux linkage trajectory in two methods. (a) PDC. (b) FSTMC-PDC.

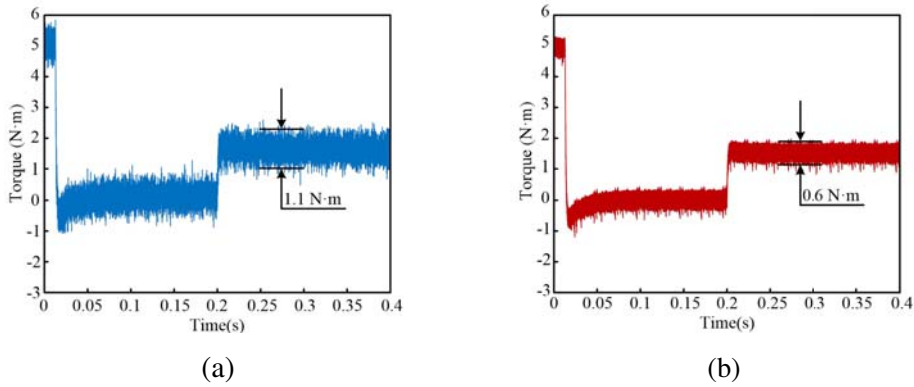


Figure 7. Torque waveforms in two methods. (a) PDC. (b) FSTMC-PDC.

PDC. The torque of the FSTMC-PDC changes about ± 0.3 N·m, which is 45% lower than that of the PDC. The results show that the torque ripple and flux ripple of the proposed FSTMC-PDC are small, which can obviously weaken the chattering phenomenon of the system and improve the speed regulation performance of the PMA-BSynRM.

Figure 8 shows the radial displacements in the x - and y -directions when the motor is set at the same offset position. In FSTMC-PDC system, the times required for the rotor to return to the balanced position in the x - and y -directions are 0.02 s and 0.03 s, and the displacement overshoots are about 0.045 mm and 0.025 mm, respectively. Compared to traditional PDC, the response speed is increased by 52.4% and 44.4%, and the displacement fluctuation is reduced by 43.8% and 58.3%. It proves that the FSTMC-PDC has faster response speed and smaller displacement fluctuations. This shows that the

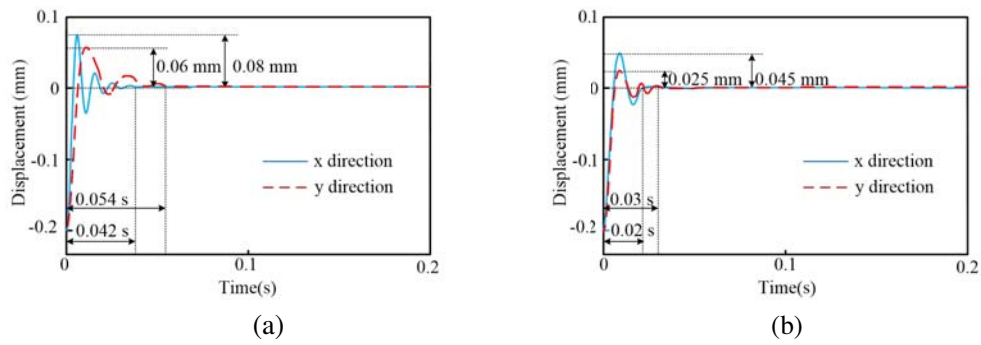


Figure 8. Radial displacement in the x -direction and y -direction in two methods. (a) PDC. (b) FSTMC-PDC.

suspension process of PMA-BSynRM is more stable and has high control accuracy due to the addition of FSTMC.

5. EXPERIMENTAL VERIFICATION

In order to validate the effectiveness of the proposed control strategy in this paper, experimental tests are carried out on PMA-BSynRM drive platform. The experimental platform based on FSTMC-PDC is shown in Figure 9. TMS320F2812 is used to implement the control algorithm.

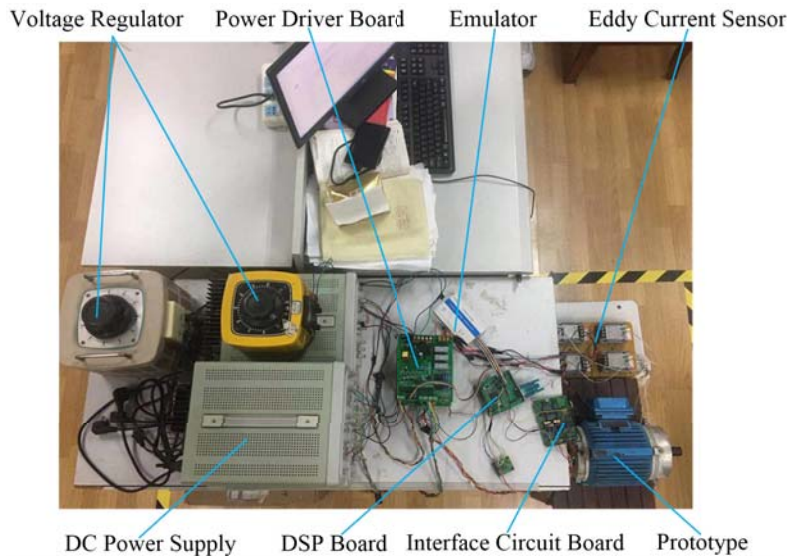


Figure 9. Experimental platform.

Figure 10 shows the radial displacements in the x - and y -directions when the speed accelerates from 2000 r/min to 3000 r/min. Obviously, the speed fluctuation of FSTMC-PDC is smaller than that of PDC. In PDC system, the rotor returns to the balanced position again after 110 ms. The recovery time of FSTMC-PDC is 70 ms, which is reduced by 37.7%.

Figure 11 shows the displacement waveforms of disturbance test for the proposed method. When motor operates steadily at 1500 r/min, the shaft is suddenly knocked. The maximum displacements in two methods in the y direction are 63 μm and 32 μm , respectively. The experimental results show that the proposed FSTMC-PDC has smaller displacement fluctuation and better anti-interference performance than PDC.

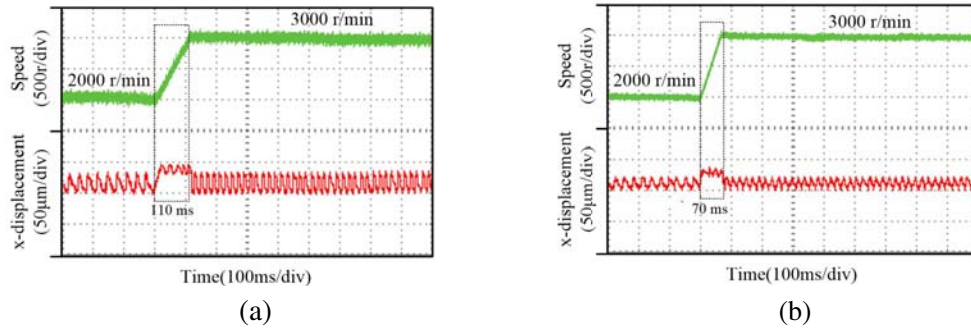


Figure 10. Radial displacement in the y direction in two methods. (a) PDC. (b) FSTMC-PDC.

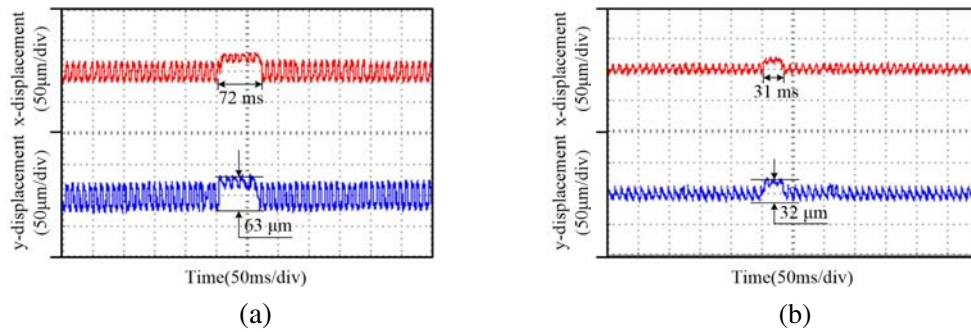


Figure 11. Radial displacement in the y direction in two methods. (a) PDC. (b) FSTMC-PDC.

6. CONCLUSION

In this paper, a fractional super twisting sliding mode controller is used to replace the hysteresis comparator in the traditional predictive direct control, which solves the chattering problem and greatly improves the accuracy and stability of the control system. The simulated and experimental results show that the designed control system can not only meet the real time control requirements of PMA-BSynRM, but also have high suspension force control accuracy and good speed regulation performance. The flux ripple and speed ripple decrease significantly; the torque fluctuation decreases from 0.55 N·m to 0.3 N·m; and the displacement overshoots decrease by 43.8% and 58.3%, respectively. The control algorithm proposed in this paper is universal and has certain reference value for other types of bearingless motor system control.

ACKNOWLEDGMENT

This work was supported by National Natural Science Foundation of China (61973144), and the Priority Academic Program Development of Jiangsu Higher Education Institution (PAPD-2018-87).

REFERENCES

1. Zhu, H.-Q., and Y. Xu, "Permanent magnet parameter design and performance analysis of bearingless flux switching permanent magnet motor," *IEEE Transactions on Industrial Electronics*, Vol. 68, No. 5, 4153–4163, 2021.
2. Ding, H.-F., H.-Q. Zhu, and Y.-Z. Hua, "Optimization design of bearingless synchronous reluctance motor," *IEEE Transactions on Applied Superconductivity*, Vol. 28, No. 3, 1–5, 2018.
3. Chiba, A., T. Fukao, O. Ichikawa, et al., *Magnetic Bearings and Bearingless Drives*, 238–250, Elsevier Newnes Press, Boston, 2005.

4. Hu, W.-C., Y.-C. Li, Z.-B. Yang, et al., "Direct torque control of bearingless synchronous reluctance motor," *Applied Mechanics and Materials*, Vol. 25, No. 150, 36–39, 2012.
5. Hu, W.-C., Y.-C. Li, H.-Q. Zhu, et al., "Direct radial suspension force control algorithm of bearingless synchronous reluctance motor," *Advance Electrical and Electronics Engineering*, Vol. 23, No. 87, 401–408, 2011.
6. Ban, F., G.-K. Lian, J.-H. Zhang, et al., "Study on a novel predictive torque control strategy based on the finite control set for PMSM," *IEEE Transactions on Applied Superconductivity*, Vol. 29, No. 2, 1–6, 2019.
7. Kim, S.-J., J. Park, and D.-H. Lee, "Zero voltage vector - based predictive direct torque control for PMSM," *IEEE Student Conference on Electric Machines and Systems*, 1–6, Busan, Korea (South), 2019.
8. Wang, X.-Q., Z. Wang, Z.-X. Xu, et al., "Optimization of torque tracking performance for direct-torque-controlled PMSM drives with composite torque regulator," *IEEE Transactions on Industrial Electronics*, Vol. 67, No. 12, 10095–10108, 2020.
9. Nikzad, M. R., B. Asaei, and O. Ahmadi, "Discrete duty-cycle-control method for direct torque control of induction motor drives with model predictive solution," *IEEE Transactions on Power Electronics*, Vol. 33, No. 3, 2317–2329, 2018.
10. Liu, Q. and K. Hameyer, "Torque ripple minimization for direct torque control of PMSM with modified FCSMPC," *IEEE Transactions on Industry Applications*, Vol. 52, No. 6, 4855–4864, 2016.
11. Cheema, M. A., J. E. Fletcher, M. Farshadnia, et al., "Sliding mode based combined speed and direct thrust force control of linear permanent magnet synchronous motors with first-order plus integral sliding condition," *IEEE Transactions on Power Electronics*, Vol. 34, No. 3, 2526–2538, 2019.
12. Ammar, A., T. Ameid, Y. Azzoug, et al., "Implementation of sliding mode based-direct flux and torque control for induction motor drive with efficiency optimization," *International Conference on Advanced Electrical Engineering*, 1–6, Algiers, Algeria, 2019.
13. Sun, X., J. Wu, G. Lei, et al., "Torque ripple reduction of SRM drive using improved direct torque control with sliding mode controller and observer," *IEEE Transactions on Industrial Electronics*, Vol. 1, No. 1, 21–32, 2020.
14. Chen, S. Z., N. C. Cheung, K. C. Wong, et al., "Integral sliding-mode direct torque control of doubly-fed induction generators under unbalanced grid voltage," *IEEE Transactions on Energy Conversion*, Vol. 25, No. 2, 356–368, 2010.
15. Sami, I., S. Ullah, A. Basit, et al., "Integral super twisting sliding mode based sensorless predictive torque control of induction motor," *IEEE Access*, Vol. 8, 186740–186755, 2020.
16. Hua, Y.-Z., H.-Q. Zhu, and Z.-H. Zhao, "Direct control of bearingless permanent magnet slice motor based on stator flux observer," *IEEE Student Conference on Electric Machines and Systems*, 1–5, Huzhou, China, 2018.
17. Mao, S., H. Tao, and Z. Zheng, "Sensorless control of induction motors based on fractional-order linear super-twisting sliding mode observer with flux linkage compensation," *IEEE Access*, Vol. 8, 172308–172317, 2020.
18. Huang, J.-C., Q.-H. Xu, X.-X. Shi, et al., "Direct torque control of PMSM based on fractional order sliding mode variable structure and space vector pulse width modulation," *Proceedings of the 33rd Chinese Control Conference*, 8097–8101, Nanjing, China, 2014.